

Maturation of hematopoietic stem cells from prehematopoietic stem cells is accompanied by up-regulation of PD-L1

Joanna Tober,^{1,2*} Marijke M.W. Maijenburg,^{1,2*} Yan Li,^{1,2} Long Gao,^{3,4,5} Brandon K. Hadland,^{6,7} Peng Gao,⁴ Kodai Minoura,^{1,2} Irwin D. Bernstein,^{6,7} Kai Tan,^{2,3,4} and Nancy A. Speck^{1,2}

¹Abramson Family Cancer Research Institute, ²Department of Cell and Developmental Biology, and ³Department of Pediatrics, University of Pennsylvania, Philadelphia, PA

⁴Department of Biomedical and Health Informatics, Children's Hospital of Philadelphia, Philadelphia, PA

⁵Department of Biomedical Engineering, University of Iowa, Iowa City, IA

⁶Clinical Research Division, Fred Hutchinson Cancer Research Center, Seattle, WA

⁷Department of Pediatrics, University of Washington, Seattle, WA

Hematopoietic stem cells (HSCs) mature from pre-HSCs that originate in the major arteries of the embryo. To identify HSCs from in vitro sources, it will be necessary to refine markers of HSCs matured ex vivo. We purified and compared the transcriptomes of pre-HSCs, HSCs matured ex vivo, and fetal liver HSCs. We found that HSC maturation in vivo or ex vivo is accompanied by the down-regulation of genes involved in embryonic development and vasculogenesis, and up-regulation of genes involved in hematopoietic organ development, lymphoid development, and immune responses. Ex vivo matured HSCs more closely resemble fetal liver HSCs than pre-HSCs, but are not their molecular equivalents. We show that ex vivo-matured and fetal liver HSCs express programmed death ligand 1 (PD-L1). PD-L1 does not mark all pre-HSCs, but cell surface PD-L1 was present on HSCs matured ex vivo. PD-L1 signaling is not required for engraftment of embryonic HSCs. Hence, up-regulation of PD-L1 is a correlate of, but not a requirement for, HSC maturation.

INTRODUCTION

Hematopoietic stem cells (HSCs) and earlier populations of committed hematopoietic progenitors are formed during embryogenesis from specialized endothelial cells called hemogenic endothelium (Zovein et al., 2008; Chen et al., 2009; Eilken et al., 2009; Lancrin et al., 2009; Bertrand et al., 2010; Boisset et al., 2010; Kissa and Herbomel, 2010). During differentiation from hemogenic endothelium, hematopoietic stem and progenitor cells (HSPCs) accumulate within clusters of vascular-endothelial cadherin-positive (VEC⁺) CD31⁺Kit⁺ cells in the aorta/gonad/mesonephros (AGM) region, umbilical and vitelline arteries, and yolk sac (Taoudi et al., 2008; Yokomizo and Dzierzak, 2010; Frame et al., 2016). The peak of cluster formation is at embryonic day (E) 10.5 in the mouse embryo, at which time there are hundreds of cluster cells in the AGM region (Yokomizo and Dzierzak, 2010), but only 0.03 functional HSCs (Müller et al., 1994; Yokomizo and Dzierzak, 2010). Between E11.5 and E12.5, the number of HSCs expands from one to three in the AGM region, and to ~50–100 in the fetal liver (FL; Kumaravelu et al., 2002; Gekas et al., 2005). Most of this expansion is from the maturation of pre-HSCs into functional HSCs in the FL (Taoudi et al., 2008; Kieusseian et al., 2012). Indeed, quantitation of HSCs

and pre-HSCs revealed that the number of HSCs in the E12.5 FL correlated with the number of pre-HSCs present 1 d earlier in the AGM region, umbilical, and vitelline arteries (AUV; Rybtsov et al., 2016).

Pre-HSC to HSC maturation can be replicated ex vivo by culturing AGM regions as explants for several days (Medvinsky and Dzierzak, 1996; Taoudi et al., 2008). Pre-HSC to HSC maturation can also be achieved by culturing disaggregated cells from the AGM region as reagggregates with OP9 stromal cells, on monolayers of endothelial cells expressing an activated form of Akt (Akt-EC), or on OP9 stromal cells expressing the Notch ligand delta-like 1 (Taoudi et al., 2008; Rybtsov et al., 2011, 2014; Hadland et al., 2015; Zhou et al., 2016). The last three procedures allow for the purification of specific populations of cells from the AGM region to determine which cell surface markers are expressed on pre-HSCs. Using this approach, Rybtsov et al. (2011) identified two populations of pre-HSCs based on expression of VEC and CD45. The first pre-HSCs detected at E10.5 were VEC⁺CD45⁻ (type I pre-HSCs; Rybtsov et al., 2011). At E11.5, in addition to type I pre-HSCs, a second type of pre-HSC (type II) appears that is VEC⁺CD45⁺. Both type I and type II pre-HSCs are Kit⁺ (Taoudi et al., 2008; Rybtsov et al., 2011, 2014). More

Dr. Maijenburg died on November 7, 2017.

*J. Tober and M.M.W. Maijenburg contributed equally to this paper.

Correspondence to Kai Tan: tank1@email.chop.edu; Nancy A. Speck: nancyas@mail.med.upenn.edu

© 2018 Tober et al. This article is distributed under the terms of an Attribution-Noncommercial-Share Alike-No Mirror Sites license for the first six months after the publication date (see <http://www.rupress.org/terms/>). After six months it is available under a Creative Commons License (Attribution-Noncommercial-Share Alike 4.0 International license, as described at <https://creativecommons.org/licenses/by-nc-sa/4.0/>).



recently, it was shown that both type I and type II pre-HSCs are CD201^{hi}, and type II pre-HSCs are CD27⁺ (Zhou et al., 2016; Li et al., 2017). The first HSCs to emerge in the embryo, as assayed by directly transplanting AGM regions, share a type II VEC⁺CD45⁺CD27⁺ pre-HSC immunophenotype (North et al., 2002; Taoudi et al., 2005; Li et al., 2017).

Protocols to produce HSCs ex vivo require generating pre-HSCs from hemogenic endothelium, and then maturing pre-HSCs into HSCs. Here we examined the molecular changes accompanying the process of pre-HSC to HSC maturation in vivo and ex vivo. We identified the immune checkpoint molecule programmed death ligand 1 (PD-L1) as a new marker for HSCs that have recently matured from pre-HSCs.

RESULTS

Purification of pre-HSCs

We determined whether type I and type II pre-HSCs could be enriched using GFP expressed from a *Ly6a:GFP* transgene, which marks ~20% of hematopoietic cluster cells and all HSCs in the AUV (de Bruijn et al., 2002; Li et al., 2014). We sorted type I (VEC⁺CD45⁻) and type II (VEC⁺CD45⁺) pre-HSCs from the AUV of E11.5 *Ly6a:GFP* transgenic embryos and fractionated them based on *Ly6a:GFP* expression (Fig. 1, A and B). *Ly6a:GFP*⁺ cells represented 20% of the VEC⁺CD45⁺ population and 30% of the VEC⁺CD45⁻ population (Fig. 1 C). The four populations were reaggregated with OP9 stromal cells and cultured as explants for 4 d, then dissociated and transplanted into lethally irradiated adult recipient mice. Only OP9 reaggregate cultures established with *Ly6a:GFP*⁺ fractions of VEC⁺CD45⁺ and VEC⁺CD45⁻ cells contained long-term repopulating HSCs (Fig. 1 D). The donor cells contributed to both lymphoid and myeloid lineage cells and phenotypic long-term repopulating HSCs (CD150⁺CD48⁻ lineage-negative, Sca1⁺Kit⁺ [LSK]) in the bone marrow (BM), and donor HSCs from the primary transplant recipient successfully engrafted secondary recipients (not depicted). Therefore, all type I and type II pre-HSCs at E11.5 are *Ly6a:GFP*⁺.

We next examined whether *Ly6a:GFP* expression could be used to isolate pre-HSCs before E11.5. It was shown that *Ly6a:GFP* expression does not faithfully mark E10.0–E10.5 pre-HSCs when assayed by direct transplantation into neonatal recipients (Boisset et al., 2015). We assessed whether the same was true for pre-HSCs matured ex vivo. To mature E10.0–E10.5 pre-HSCs, we switched to a more efficient system than reaggregate cultures that involves coculturing with AGM-derived endothelial cells that are infected with a lentivirus expressing myristoylated Akt (Akt-EC; Kobayashi et al., 2010; Hadland et al., 2015). We first examined whether coculturing pre-HSCs isolated from E11.5 embryos on Akt-ECs yielded similar results as reaggregate explants. The *Ly6a:GFP*⁺ fractions of both VEC⁺CD45⁻ and VEC⁺CD45⁺ pre-HSC populations from E11.5 embryos cultured on Akt-EC contained all the pre-HSC activity (Fig. 1 E), identical to the result obtained using OP9 reaggregate

explants (Fig. 1 D), although engraftment by HSCs matured on Akt-ECs was more robust. At E10.0 (30–35 somite pairs), all pre-HSCs were in the VEC⁺CD45⁻ population (type I), as reported previously (Rybtsov et al., 2011). However, unlike at E11.5, when all pre-HSCs are *Ly6a:GFP*⁺, at E10.0, pre-HSCs were split between the *Ly6a:GFP*⁺ and *Ly6a:GFP*⁻ fractions (Fig. 1 G). At E10.5 (34–38 somite pairs), pre-HSCs were in both the VEC⁺CD45⁻ and VEC⁺CD45⁺ populations, and were enriched in, although did not exclusively segregate to, the *Ly6a:GFP*⁺ fractions (Fig. 1 H). Therefore, *Ly6a:GFP* expression enriches for pre-HSCs beginning at E10.5, and marks all pre-HSCs at E11.5.

Explant HSCs are in the CD48⁻ LSK population

To study the molecular changes that take place as pre-HSCs mature into HSCs ex vivo, we refined the cell surface phenotype of HSCs matured from pre-HSCs in explant cultures (HSC ex vivo, referred to here as HSC^{ex}). Long-term repopulating HSCs from the FL and BM are highly enriched in the CD150⁺CD48⁻ LSK population, whereas functional HSCs in the E11.5 AUV are CD150⁻CD48⁻Sca1⁺Kit⁺ (Sánchez et al., 1996; de Bruijn et al., 2002; North et al., 2002; Kiel et al., 2005; Kim et al., 2006; McKinney-Freeman et al., 2009). To determine whether CD150 expression marks HSC^{ex}, we explanted AUVs from E11.5 WT embryos, fractionated CD45⁺ LSK cells into four populations based on CD150 and CD48 expression, and transplanted the cells into lethally irradiated recipients (Fig. 2). CD150⁻CD48⁺ cells contributed to peripheral blood (PB) B and T cells, but robust multilineage engraftment was observed only in animals transplanted with CD48⁻ LSK cells (Fig. 2 C). Both the CD150⁺ and CD150⁻ fractions of CD48⁻ LSK cells engrafted, with significantly higher levels of donor contribution obtained with the CD150⁻CD48⁻ LSK population. We conclude that HSC^{ex} are in transition between AUV and FL HSCs, in that some have acquired CD150 expression whereas others are still CD150⁻.

Molecular comparison of pre-HSCs, HSC^{ex}, and FL HSCs

We performed RNA-Seq to compare the molecular profiles of E11.5 pre-HSCs, HSC^{ex}, and FL HSCs. We sorted pre-HSCs as CD31⁺VEC⁺ESAM⁺Kit⁺*Ly6a:GFP*⁺ cells, which contain both type I and type II pre-HSCs. As ESAM had not previously been demonstrated to mark pre-HSCs, we first confirmed that all pre-HSCs are in the ESAM⁺ population of CD31⁺VEC⁺Kit⁺*Ly6a:GFP*⁺ cells (Fig. 2, D and E). HSC^{ex} (CD48⁻ LSK) were purified from E11.5 AUV that had been cultured as explants for 4 d, and FL HSCs (CD48⁻CD150⁺ LSK) from E14.5 embryos. In total, 5294 differentially expressed genes (DEGs) were identified between pre-HSCs, HSC^{ex}, and FL HSCs (Fig. 3 A and Fig. S1, A and B). A principal component analysis (PCA) showed the three top principal components accounted for 80% of the variance in gene expression (Fig. S1 C). The PCA segregated pre-HSCs, HSC^{ex}, and FL HSCs into three distinct groups (Fig. 3 B and Fig. S1 D). HSC^{ex} and FL HSCs, although

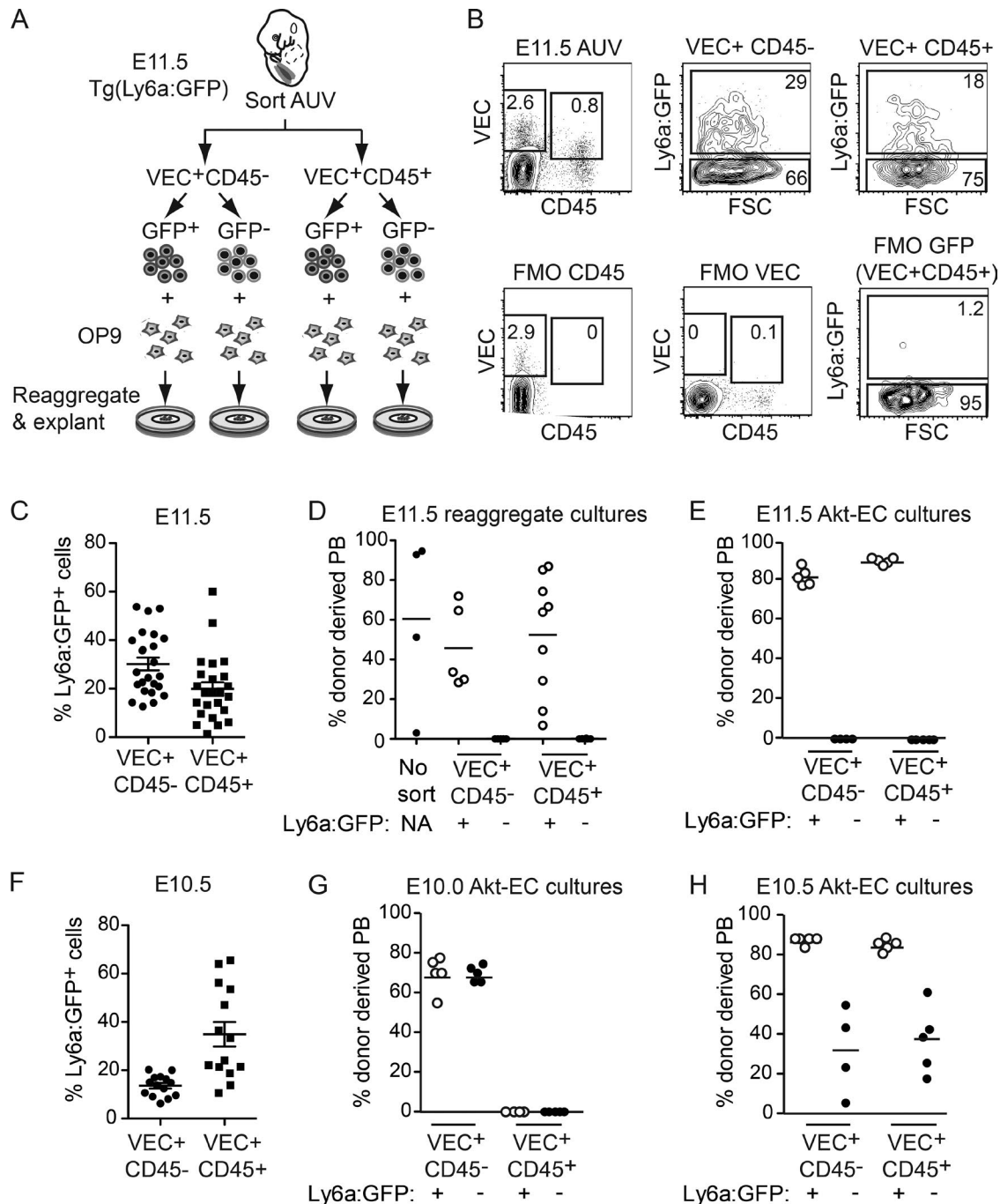


Figure 1. **Ly6a:GFP** exclusively marks pre-HSCs at E11.5. **(A)** Dissected AUV from *Ly6a:GFP* transgenic embryos were sorted into VEC⁺CD45⁺GFP^{+/−} and VEC⁺CD45[−]GFP^{+/−} populations. Sorted populations were cultured as reaggrenates with OP9 cells for 4 d. **(B)** Representative sort plots and fluor-minus-one (FMO) controls for E11.5 *Ly6a:GFP*⁺ cells. Percentages of gated FACS populations are shown. **(C)** The percentage (error bars, 5th to 95th percentile) of *Ly6a:GFP*⁺ cells in the VEC⁺CD45⁺ and VEC⁺CD45[−] populations at E11.5. Data were compiled from 24 independent experiments. **(D)** After coculturing for 4 d, OP9 reaggrenates were dissociated, and one embryo equivalent (ee) of cells was transplanted into lethally irradiated recipient mice. Data represent the mean percent donor contribution (CD45.2⁺ cells) to PB cells for individual transplant recipients ($n = 14$ each for type I and type II). "No sort" represents cells from the explant transplanted without sorting ($n = 4$); NA, not applicable. Data were compiled from three separate experiments. **(E)** Mean engraftment of adult mice with 1 ee of E11.5 pre-HSCs matured into HSCs on Akt-ECs. Data were compiled from five mice per condition in one experiment. **(F)** Percentage \pm standard deviation of *Ly6a:GFP*⁺ cells in the VEC⁺CD45⁺ and VEC⁺CD45[−] populations at E10.5. Data were compiled from 14 independent experiments. **(G and H)** Mean contribution to PB from 1 ee of E10.0 (30–35 sp) and E10.5 (34–38 sp) pre-HSCs matured into HSCs on Akt-ECs. Data were compiled from five mice per condition in two independent experiments. All transplant experiments were evaluated at 16 wk.

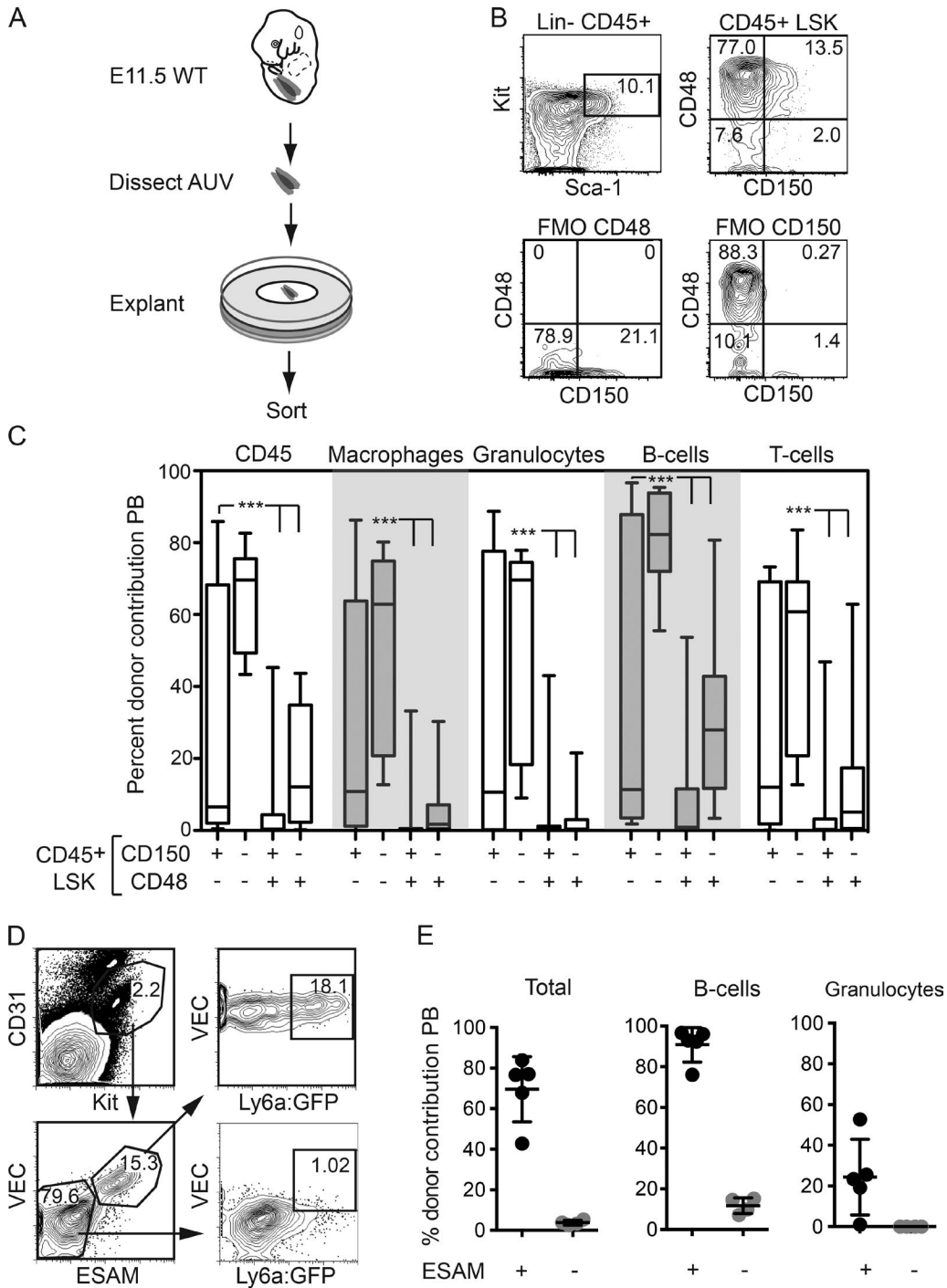


Figure 2. **Refinement of HSC^{ex} and pre-HSCs for molecular profiling.** (A) Dissected AUV from WT embryos were explanted for 4 d, and the CD45⁺ LSK population sorted based on CD48 and CD150 expression. One ee of each population was transplanted into recipient mice. (B) Representative sort plots with FMO controls. (C) Donor contribution to PB in transplant recipients. Data were compiled from three independent experiments; *n* = 4 recipients for each population. Animals transplanted with CD48⁻CD150⁻ cells had significantly higher donor contribution to CD45⁺ and B cells compared with animals transplanted with other sorted populations, and to macrophages, granulocytes, and T cells compared with animals transplanted with CD150⁺CD48⁺ or CD150⁻CD48⁺ cells (***, *P* < 0.0001). Error bars show minimum to maximum values. One-way ANOVA and Tukey's multiple comparison tests. (D) Representative sort plots of pre-HSCs from E11.5 AUV. (E) Contribution in individual transplant recipients of 1 ee of pre-HSCs (ESAM⁺ [5 recipients] and ESAM⁻ [4 recipients] populations of CD31⁺VEC⁺Kit⁺Ly6a:GFP⁺ cells) to total PB cells (Total), B cells, and granulocytes (mean ± SD). All engraftment was determined at 16 wk. Percentages of gated FACS populations are shown.

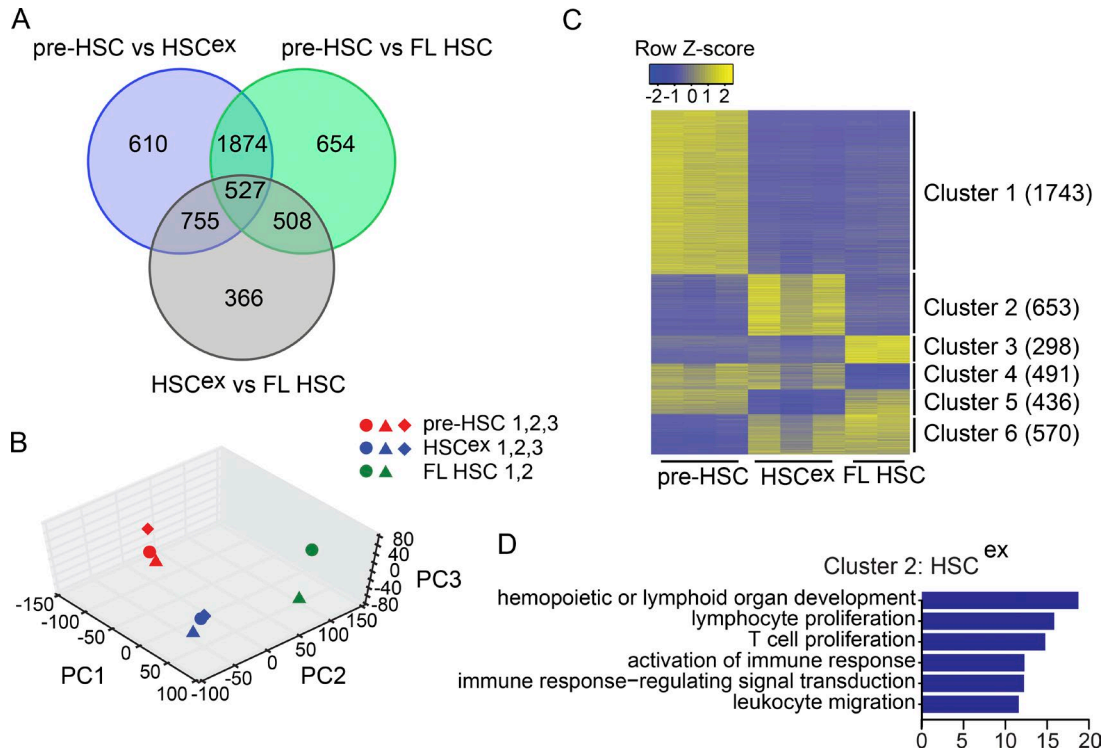


Figure 3. RNA-Seq analysis of pre-HSCs, HSC^{ex}, and FL HSCs. (A) Venn diagram of DEGs from pairwise comparisons of pre-HSC, HSC^{ex} and FL HSCs. Pre-HSCs were sorted as CD31⁺VEC⁺ESAM⁺Kit⁺Ly6a⁻GFP⁺ cells, HSC^{ex} as CD48⁻ LSK, and FL HSCs as CD48⁻CD150⁺ LSK cells. DEGs were identified using a false discovery rate cutoff <0.05 and a fold change cutoff >2. (B) PCA (see also Fig. S1). The top 5,000 genes with the largest expression variance across samples were used for the analysis. (C) Expression clusters defined using consensus clustering and DEGs (see also Fig. S2). Color indicates row-wise normalized expression levels. Numbers (n) indicate number of genes in each cluster. (D) GO terms associated with genes more highly expressed in HSC^{ex} than pre-HSCs and FL HSCs (see also Fig. S3).

distinct, were more closely related to each other than either was to pre-HSCs. Potential reasons for the distinct molecular signatures of HSC^{ex} and FL HSCs are that the HSC^{ex} population contained other contaminating progenitors, as will be addressed later, and/or that the ex vivo culture conditions result in HSCs with a different molecular profile than those in their normal in vivo niche.

Using consensus clustering and the set of differentially expressed genes, we defined six clusters of expression profiles (Fig. 3 C, Fig. S2, and Table S1). Clusters 1–3 consist of genes that are most highly expressed in pre-HSCs, HSC^{ex}, or FL HSCs, respectively (Fig. 3 C and Fig. S2). Clusters 4–6 consist of genes that are more highly expressed in two of the three cell types. Genes in cluster 1 that were most highly expressed in pre-HSCs were associated with gene ontology (GO) terms related to “vascular morphogenesis” and “embryonic organ development” (Fig. S3 A). The preponderance of GO terms related to embryonic organ development indicates that pre-HSCs have not yet extinguished the expression of genes associated with other cell fates, and GO terms related to vasculogenesis reflect their recent identity as hemogenic endothelial cells. On the other hand, many significant GO terms associated with genes in cluster 2 (more highly ex-

pressed in HSC^{ex} than in pre-HSCs or FL HSCs; Fig. 3 D and Fig. S3 B) and in cluster 6 (higher in both HSC^{ex} and FL HSCs relative to pre-HSCs; Fig. S3 F) were associated with lymphoid differentiation or response. Thus, the maturation of pre-HSCs to HSCs involves up-regulation of a hematopoietic and particularly lymphoid program, and down-regulation of an endothelial program, as reported by others (Kim et al., 2006; McKinney-Freeman et al., 2009; Zhou et al., 2016).

The CD48⁻ LSK population from AUV explant cultures contains cells with lymphoid markers that are not HSCs

We extracted a list of genes encoding cell surface receptors that were more highly expressed in HSC^{ex} (CD48⁻ LSK cells) compared with pre-HSCs, to identify cell surface markers that could potentially be used to further purify the functional HSC^{ex} in this population (Table 1). The list contained many genes expressed in lymphocytes, including subunits of the IL receptors (*Il2ra*, *Ilr2b*, *Il18r*, *Il12rb1*, *Il7r*), components of the TCR (*Trbc1*, *Tcr γ -C1*), and chemokine receptors (*Ccr7*, *Ccr8*, *Ccr9*, *Cxcr5*). Also on the list were several immune checkpoint or immune suppressor molecules, including *Cd300lf*, *Cd96*, *Cd69*, *Cd244*, and *Cd274* (PD-L1). We examined the expression of several of these markers on CD48⁻

LSK cells from AUV explants, and found that up to 20% of CD48⁻ LSK cells were positive for one or more lymphoid marker (Fig. 4 A). The prevalence of lymphoid marker expression in CD48⁻ LSK cells suggested that either the HSC^{ex} population is primed toward the lymphoid lineage, or that it is contaminated by committed lymphoid progenitors. To determine whether CD48⁻ LSK cells expressing lymphoid markers contained functional HSC^{ex}, we sorted CD48⁻ LSK cells from AUV explant cultures based on expression of the IL-7 receptor (IL-7R; CD127, encoded by *Il7r*), which marks lymphoid-primed multipotent progenitors, common lymphoid progenitors, and other lymphocyte populations (Kondo et al., 1997; Akashi et al., 2000; Kawamoto et al., 2000; Böiers et al., 2013), and transplanted the cells into mice (Fig. 4, B and C). All HSC^{ex} were in the IL-7R⁻CD48⁻ LSK fraction. We examined the IL-7R⁺CD48⁻ LSK population for lymphoid potential by culturing cells on OP9 and OP9-DL1, and determined that it contained progenitors with B (OP9) and T (OP9-DL1) lymphoid potential (not depicted). Antibodies to IL-7R could therefore be used to exclude contaminating lymphoid progenitors from the CD48⁻ LSK population in order to obtain a more pure population of functional HSC^{ex}.

PD-L1 is expressed on HSC^{ex} and FL HSCs

To identify positive cell surface markers for HSC^{ex}, we focused on genes in cluster 6 that were up-regulated on both HSC^{ex} and FL HSCs. One candidate was PD-L1 (also known as CD274), a transmembrane receptor that binds PD-1 on T lymphocytes and delivers an inhibitory signal to prevent TCR-mediated T cell activation (Zheng et al., 2011; Riella et al., 2012). We sorted cells from AUV explants based on PD-L1 expression, and showed that functional HSCs were enriched in the PD-L1⁺ fractions of both CD48⁻ LSK cells (Fig. 4, D and E) and IL7R⁻CD48⁻ LSK cells (Fig. 4 F and Fig S4, A and B). BM from primary recipients of PD-L1⁺IL7R⁻CD48⁻ LSK HSC^{ex} cells that were transplanted into secondary recipients contributed to long-term reconstitution of PB, and to BM HSPCs (Fig. S4, B and C). PD-L1⁺IL-7R⁻ cells constituted ~30% of the CD48⁻ LSK population in AUV explant cultures (Fig. 4 G); thus, the combination of PD-L1 and IL-7R as positive and negative markers, respectively, can be used to further enrich functional HSC^{ex} from ex vivo cultures.

We also determined whether PD-L1 marks HSCs in the E11.5 AUV by direct transplantation of VEC⁺ AUV cells sorted based on PD-L1 expression (Fig. 5, A–C). HSCs in the E11.5 AUV were in both the PD-L1⁺ and PD-L1⁻ fractions of VEC⁺ cells (Fig. 5 C), and therefore PD-L1 does not exclusively mark HSCs in the E11.5 AUV. We next asked whether PD-L1 marks HSCs in the FL. We sorted PDL1⁺ and PD-L1⁻ fractions of Lin⁻IL-7R⁻ FL cells from E11.5, E12.5, and E14.5 fetuses and transplanted the cells into irradiated recipients (Fig. 5 E). Most FL HSCs at all three stages were PD-L1⁺. Thus, PD-L1 marks most HSCs that have matured in vivo in the FL.

We determined whether PD-L1 marks pre-HSCs by fractionating VEC⁺ cells from the AUV of E10.0 (30–35 so-

Table 1. Cell surface markers up-regulated on HSC^{ex} vs. preHSCs

Gene symbol	Fold change	P-values
<i>Il2ra</i>	7751.7	5.57E-17
<i>Tcrg-C1</i>	7127.9	4.14E-14
<i>Trbc1</i>	4995.8	3.62E-11
<i>Ifitm6</i>	3444.8	1.39E-07
<i>Itgb2l</i>	2727.0	7.60E-06
<i>Cd177</i>	2402.3	5.81E-05
<i>Il2rb</i>	1126.8	1.03E-55
<i>Amica1</i>	1097.1	6.90E-11
<i>Il1r2</i>	464.6	1.60E-152
<i>Il18r1</i>	380.2	2.87E-05
<i>Ccr9</i>	339.1	2.90E-71
<i>Cd7</i>	250.9	1.30E-46
<i>Cd96</i>	163.2	2.02E-10
<i>Il1rl1^a</i>	120.4	4.85E-88
<i>Cd244</i>	119.7	1.62E-63
<i>Ccr8</i>	112.0	2.75E-07
<i>Cd200r3</i>	109.9	2.37E-32
<i>Itgb7^a</i>	83.5	2.01E-148
<i>Il12rb1^a</i>	53.3	3.27E-12
<i>Il7r</i>	52.8	7.32E-25
<i>Cd69</i>	52.4	1.40E-104
<i>Ccr7</i>	46.0	1.71E-09
<i>Cd74</i>	42.5	2.76E-52
<i>Cdh17</i>	30.1	5.59E-18
<i>Ifitm1^a</i>	25.1	7.04E-94
<i>Dkk1^a</i>	18.7	7.56E-05
<i>Itgax</i>	18.6	6.32E-07
<i>Cd200r4</i>	18.3	9.21E-09
<i>Cxcr5</i>	15.0	7.53E-06
<i>Cd37^a</i>	13.1	1.79E-59
<i>Itgae</i>	12.1	4.01E-3
<i>Il9^a</i>	11.8	3.91E-07
<i>Cd300lf^a</i>	11.7	1.12E-12
<i>Cd82^a</i>	10.4	2.14E-65
<i>Itgb2^a</i>	7.9	1.20E-38
<i>Cd274 (PD-L1)^a</i>	7.5	4.07E-13
<i>Cxcr4^a</i>	6.3	1.52E-19
<i>Il1r1</i>	5.1	4.68E-27

^aAlso expressed on FL HSCs.

mite pairs [sp]) and E11.5 (46–48 sp) embryos into PD-L1 high (hi), low (lo), and negative (–) populations (Fig. 6, A and B), culturing the cells on Akt-EC to mature the pre-HSCs into HSC^{ex}, and transplanting the cultured output into recipient mice. At E10.0, all pre-HSCs were in the PD-L1^{lo} and PD-L1⁻ populations of VEC⁺ cells, and none were in the PD-L1^{hi} population (Fig. 6 C). At E11.5, pre-HSCs were split among the PD-L1^{hi}, PD-L1^{lo}, and PD-L1⁻ populations of VEC⁺ AUV cells. We examined whether PD-L1 expression specifically marked type I (VEC⁺CD45⁻) or type II (VEC⁺CD45⁺) pre-HSCs. Type I pre-HSCs were exclusively PD-L1⁻. Cells with type I markers that were PD-L1⁺ contributed only to B and T lymphocytes but not to myeloid lineage cells (Fig. 6 D), nor did they engraft secondary recipients (Fig. 6 E). Type II pre-HSCs were split between the PD-L1⁺ and PD-L1⁻ fractions (Fig. 6, D and E). In summary, type I pre-HSCs are PD-L1⁻, whereas type II pre-HSCs can be PD-L1⁺ or PD-L1⁻.

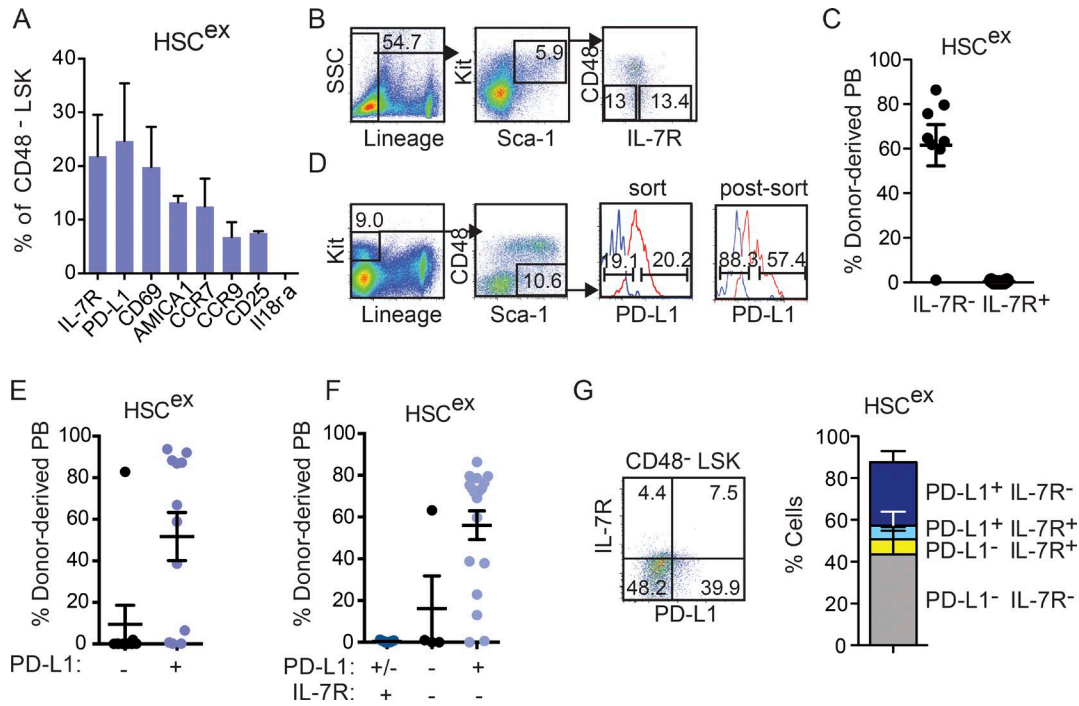


Figure 4. HSC^{ex} and FL HSCs are PD-L1⁺ IL-7R⁻. (A) Percentage (bars, 5th to 95th percentile; $n = 5$) of CD48⁻ LSK HSC^{ex} expressing various cell surface proteins, analyzed by flow cytometry. (B) FACS plots for sorting IL-7R⁺ and IL-7R⁻ fractions of CD48⁻ LSK cells. Gates were set using FMO controls (not depicted). Percentages of gated FACS populations are shown. (C) Percentage of donor-derived PB cells from 1–2 ee of the fractions sorted in B (mean \pm SD). Error data were compiled from two independent experiments; IL-7R⁻, $n = 8$; IL-7R⁺, $n = 7$. (D) FACS plots for sorting PD-L1⁺ and PD-L1⁻ CD48⁻ LSK cells from explant cultures. Left histogram: Gates in sort were set using FMO for PD-L1 (blue line). Numbers above gates are percentages of PD-L1⁺ and PD-L1⁻ cells in the sort. Right histogram: Postsort analysis of PD-L1⁺ (red) and PD-L1⁻ (blue) cells overlaid in one graph. The PD-L1 (PE) signal diminishes in the postsort; hence, many PD-L1⁺ cells shift left into the PD-L1⁻ gate. (E) Percentage \pm standard error of mean of donor-derived cells in the PB of transplant recipients of 1 ee cells sorted in D. Data were compiled from three independent experiments; PD-L1⁺, $n = 9$; PD-L1⁻, $n = 12$. (F) Percentage of donor-derived cells in PB from recipients transplanted with 1–2 ee of CD48⁻ LSK cells sorted into PD-L1⁺IL-7R⁺ ($n = 4$), PD-L1⁻IL-7R⁻ ($n = 9$), and PD-L1⁺IL-7R⁻ fractions ($n = 18$). Data were compiled from three independent experiments. (G) Proportion of CD48⁻ LSK cells expressing PD-L1 and IL-7R by flow cytometry. Data are combined from five separate flow experiments. Totals do not reach 100%, reflecting minor variability in the proportion of markers within the CD48⁻ LSK population after 4 d of culture. Percentages and standard deviation of gated FACS populations are shown. All transplant recipients were analyzed at 16 wk.

The increase in PD-L1 expression from pre-HSCs to HSC^{ex} prompted us to examine whether PD-L1⁺ HSC^{ex} differentiated from PD-L1⁻ pre-HSCs. We sorted E11.5 AUV VEC⁺ cells into PD-L1⁺ and PD-L1⁻ fractions, cultured the cells for 1 wk on Akt-EC, resorted the cells based on PD-L1 expression, and transplanted them (Fig. 6 F). Cells that were initially PD-L1⁺ and lost PD-L1 expression during ex vivo culture had no HSC^{ex} activity (Fig. 6 G). Cells that were initially PD-L1⁻ and remained PD-L1⁻ after ex vivo culture contributed to lymphoid but not to myeloid cell lineages. All populations that were PD-L1⁺ after ex vivo culture, regardless of whether they were PD-L1⁺ or PD-L1⁻ before ex vivo culture, had HSC^{ex} activity. Thus, HSC^{ex} either mature from PD-L1⁺ pre-HSCs and maintain PD-L1 expression, or differentiate from PD-L1⁻ pre-HSCs and up-regulate PD-L1 during ex vivo culture.

PD-L1 is not necessary for engraftment

We determined if PD-L1⁻ FL cells failed to engraft because they were rejected by lymphocytes in the host. We transplanted

PD-L1⁺ and PD-L1⁻ E14.5 FL cells into bisulfan-treated NOD SCID gamma (NSG) mice lacking B, T, and natural killer cells, either by retroorbital injection with splenic support cells or direct interfemoral transplant (Fig. 7 A). PD-L1⁺ donor cells reconstituted 19 of 20 NSG recipients with all lineages, contributing to 92.4% of PB cells (Fig. 7 B). In contrast, only 6 of 15 NSG recipients of PD-L1⁻ cells had donor-derived cells in their PB, 5 of which had only donor-derived lymphoid cells (Fig. 7 B). Calculating lymphoid contribution as the percentage of donor-derived B and T cells suggests that contribution of PD-L1⁻ FL cells to lymphoid lineages in NSG hosts is relatively high (30.0% of B cells, 55.5% T cells; Fig. 7 C). However, NSG hosts lack competing lymphocytes, so if instead the percentage of donor-derived lymphoid cells is calculated as a fraction of all CD45⁺ PB cells, it is apparent that the output of lymphoid cells from PD-L1 donor FL cells is much lower (11.6% B, 2.6% T; Fig. 7 D). B6.SJL (WT congenic) recipients transplanted contemporaneously with the same donor cells were engrafted only by PD-L1⁺ FL cells, and no recipients were engrafted with PD-L1⁻ cells (Fig. 7 E). Three of the 15 NSG

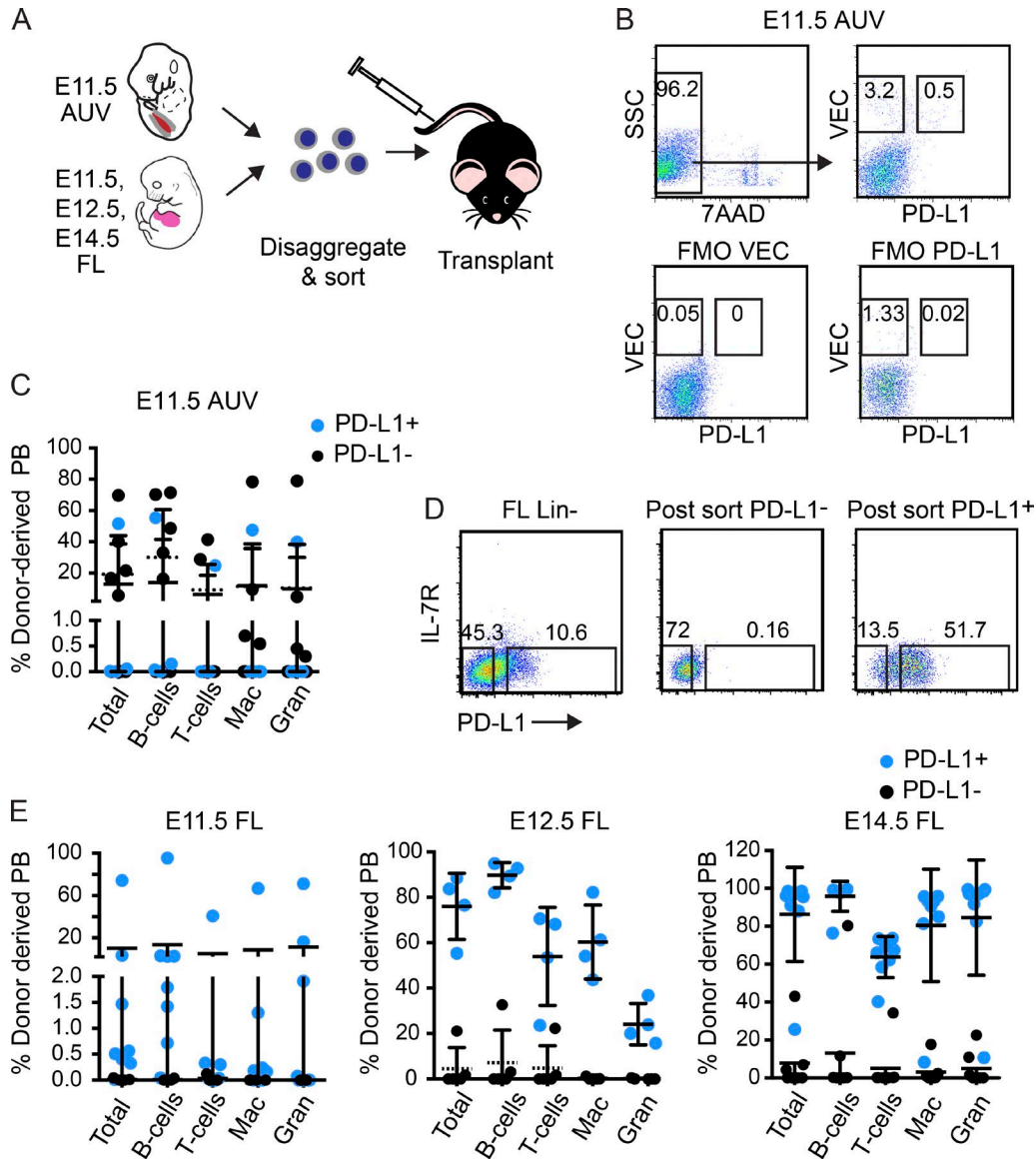


Figure 5. PD-L1 marks HSCs in the FL, but not in the AUV. (A) Schematic for direct transplantations of AUV or FL cells. **(B)** FACS sort plots of PD-L1⁺ and PD-L1⁻VEC⁺ cells from the E11.5 AUV. Plots on bottom are FMO controls. 1 ee of gated populations were transplanted. **(C)** Percentage ± standard deviation of donor-derived cells in the PB from transplanted cells sorted in B. VEC⁺PD-L1⁺, *n* = 8. VEC⁺PD-L1⁻, *n* = 13. Data are from three separate experiments. Solid horizontal line indicates mean for PD-L1⁺ cells, dotted line for PD-L1⁻ cells. **(D)** FACS plots showing sort strategy for isolating PD-L1⁺ and PD-L1⁻IL-7R⁻Lin⁻ cells from the FL for transplantation assays in E. E14.5 FL sorts and postsorts are shown. Gates were set using FMO controls (not depicted). The PD-L1 (PE) signal diminishes in the postsort; hence, many PD-L1⁺ cells shift left into the PD-L1⁻ gate. **(E)** Percentage of donor-derived cells in the PB of recipients of E11.5 (1 ee), E12.5 (1 ee), and E14.5 (5.3E4 IL7R⁻PD-L1⁺, 2.4E4 IL7R⁻PD-L1⁻) FL cells. Percentages of gated FACS populations are shown. All transplant recipients were analyzed at 16 wk. *n* = 4 experiments.

recipients of PD-L1⁻ cells contained >1% donor-derived phenotypic long-term repopulating HSCs (CD48⁻CD150⁺LSK) in their BM (Fig. 7 F), whereas no B6.SJL recipients contained >1% donor-derived CD48⁻CD150⁺LSK cells (not depicted). Hence, the lack of host lymphocytes in NSG mice allowed for limited engraftment by PD-L1⁻ FL cells. These data indicate that the PD-L1⁻ population of FL cells contains few if any HSCs capable of multilineage engraftment. Furthermore, the

inability of PD-L1⁻ FL cells to provide robust multilineage engraftment is not a result of rejection by the host immune system.

It has been proposed that the failure of embryonic pre-HSCs to engraft adult mice may be a result of rejection of immunologically unfamiliar cells by the host immune system, and it was shown that up-regulation of major histocompatibility class I molecules correlated with the ability of embryonic HSCs to engraft (Kieusseian et al.,

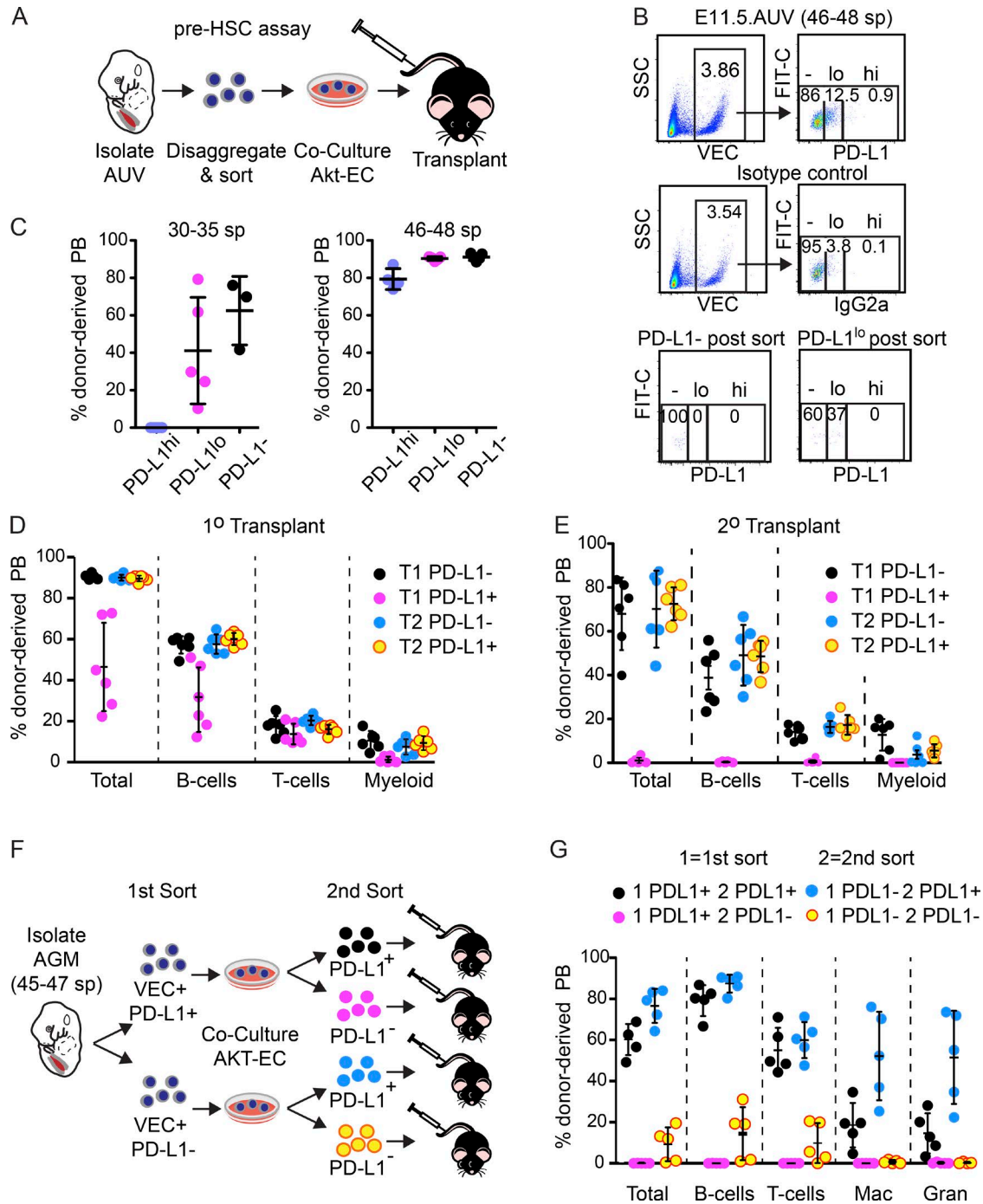


Figure 6. PD-L1 expression on pre-HSCs. (A) Schematic for pre-HSC assay. (B) FACS sorting strategy for isolation of VEC⁺PD-L1⁻, VEC⁺PD-L1^{lo}, and VEC⁺PD-L1^{hi} cells from E11.5 AUV for pre-HSC assay. Gates were set using FMO controls (not depicted). Isotype controls and postsort purity checks are shown. Percentages of gated FACS populations are shown. (C) Donor contribution to PB by VEC⁺PD-L1⁻, VEC⁺PD-L1^{lo}, and VEC⁺PD-L1^{hi} cells isolated at two different embryonic stages before Akt-EC culture (mean ± SD). 14 and 13 mice were transplanted for 30–35 sp and 46–48 sp, respectively, in two independent experiments. (D) VEC⁺CD45⁻ (type I, T1) and VEC⁺CD45⁺ (type II, T2) pre-HSCs were fractionated based on PD-L1 expression, cultured on Akt-EC, and 1 ee transplanted into recipient mice. Shown is the mean ± standard deviation of donor contribution to PB in primary (1^o) transplant recipients. (E) Secondary (2^o) transplant recipients of BM from 1^o recipients in D. Mean engraftment ± standard deviation is shown. (F) Schematic for determining whether PD-L1⁺ HSC^{ex} differentiate from PD-L1⁻ pre-HSCs. (G) Donor-derived cells in PB of recipients of PD-L1⁺ and PD-L1⁻ pre-HSCs that were cultured on Akt-EC, re-sorted for PD-L1 expression, and transplanted. Data are the mean ± standard deviation from 20 mice. All transplant recipients analyzed at 16 wk.

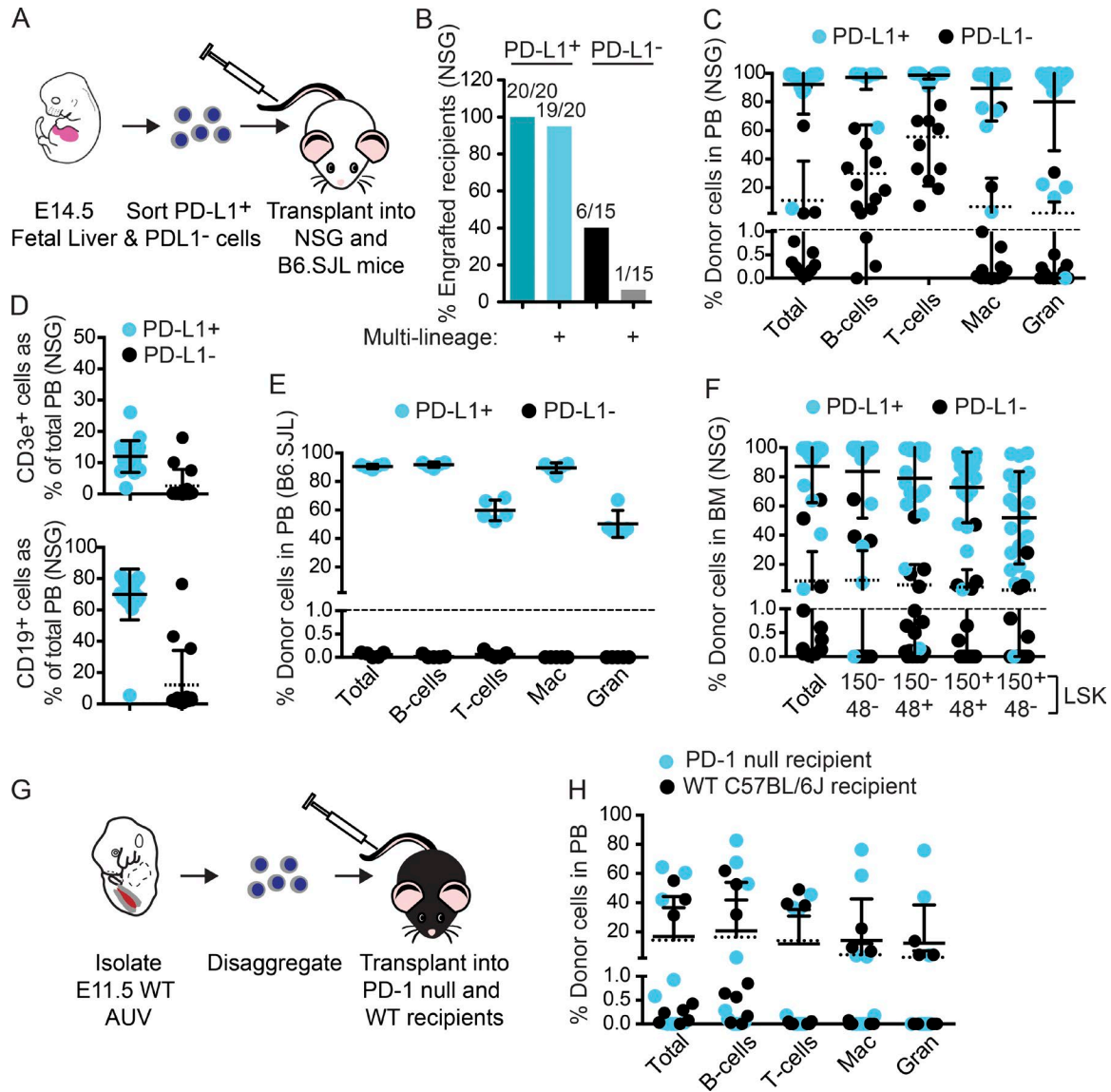


Figure 7. Engraftment in the absence of lymphocytes in the recipient, or in the absence of PD-L1:PD-1 signaling. (A) Scheme for analyzing engraftment of Lin⁻PD-L1⁺ and PD-L1⁻ FL cells in NSG mice. (B) Number of NSG recipients with engraftment, and with multilineage engraftment. 1 of 20 NSG recipients of 2E4 PD-L1⁺ FL cells and 5 of 6 recipients of 2E4 PD-L1⁻ FL cells had only lymphoid cell engraftment. Data were compiled from four separate experiments. (C) Donor contribution to total PB cells, B cells, T cells, monocytes, and granulocytes in NSG recipients. Solid horizontal lines indicate means \pm standard deviation for PD-L1⁺ cells, and dotted lines for PD-L1⁻ cells. (D) Percentage \pm standard deviation of donor-derived B (CD19⁺) and T (CD3e⁺) cells in all PB cells (donor + recipient) in NSG recipients. (E) Contribution of PD-L1⁺ and PD-L1⁻ FL cells, five mice per condition, to the PB of WT B6.SJL mice. Mean \pm standard deviation is shown. (F) Contribution of PD-L1⁺ and PD-L1⁻ FL cells to HSPCs in the BM of NSG recipients. Mean \pm standard deviation is shown. (G) Schematic for comparing engraftment of embryonic HSCs in WT and PD-1-null recipient mice. (H) Donor contribution of cells from the AUV of E11.5 WT (B6.SJL) embryos to HSPCs in the BM of WT (C57BL6/J) and PD-1-null recipient mice. Data were compiled from transplanting into 9 C57BL6/J and 10 PD-1-null recipients in two separate experiments. Mean \pm standard deviation is shown.

2012). We reasoned that if inhibition of host lymphocyte activation via PD-L1:PD-1 signaling is required for engraftment by embryonic HSCs, disrupting that axis would affect engraftment. We tested this hypothesis by transplanting HSCs from the AUV of E11.5 WT embryos into both WT and PD-1-deficient host mice. If inhibition of host lymphocyte activation through PD-1 is important

for the engraftment of embryonic HSCs, then embryonic HSCs should engraft PD-1-deficient hosts less well than they engraft WT hosts. Engraftment of E11.5 embryonic cells was equally efficient in PD-1-null and WT recipients (Fig. 7, G and H). Hence, the PD-L1:PD-1 immune checkpoint axis does not appear to be a factor impeding embryonic HSC transplantation.

DISCUSSION

The process of pre-HSC to HSC maturation is poorly understood. Cell surface and other molecular markers that can be used to identify and monitor various stages of pre-HSC to HSC maturation would facilitate efforts to understand the molecular basis of this process, and to produce HSCs *ex vivo* from embryonic stem cells, induced pluripotent stem cells, or other cell sources. Here we used the *Ly6a:GFP* transgene in conjunction with antibodies to cell surface markers on hematopoietic cluster cells to isolate and profile a population of pre-HSCs by RNA-Seq. Although the *LY6A* gene is not conserved in humans (Holmes and Stanford, 2007), we reasoned that the transcription factors and signaling pathways active in *Ly6a:GFP*⁺ mouse pre-HSCs will be conserved in human pre-HSCs. Recently, Zhou et al. (2016) performed single-cell RNA-Seq on pre-HSCs and FL and BM HSCs, using antibodies to the endothelial protein C receptor (EPCR/CD201) to refine type I and type II pre-HSC populations. Although the markers used to isolate pre-HSCs differ from those in our study, the two datasets show strong similarity in top GO terms associated with genes expressed more highly by pre-HSCs than FL HSCs, including blood vessel development and vasculogenesis.

We showed that matured HSCs (HSC^{ex} and FL HSCs) could be enriched with antibodies to PD-L1. The presence of PD-L1 on the surface of some, but not all, E11.5 AUV-resident HSCs and pre-HSCs, the expression of PD-L1 on *in vivo* FL HSCs, and the demonstration that PD-L1⁺ HSC^{ex} can differentiate from PD-L1⁻ pre-HSCs indicate that PD-L1 expression is up-regulated during HSC maturation. We previously showed that PD-L1 (*Cd274*) mRNA levels were also elevated in *Ly6a:GFP*⁺ hematopoietic cluster cells compared with *Ly6a:GFP*⁻ cells (Li et al., 2017). Likely candidates mediating the increase in PD-L1 expression are inflammatory signaling pathways. PD-L1 expression is activated by IFN- γ , and the *Cd274* promoter contains a binding site for the transcription factor IRF-1 (Lee et al., 2006). We and others showed IFN- γ signaling is active in the embryo, and positively regulates HSC and lymphoid progenitor production in both mouse and zebrafish embryos (Li et al., 2014; Sawamiphak et al., 2014). Inflammatory signaling pathway components are robustly expressed by pre-HSCs as early as E10.5 (Li et al., 2014; Kim et al., 2016). We show here that the inflammatory signature becomes more pronounced as pre-HSCs mature into FL HSCs, consistent with previous studies (Kim et al., 2016). Jak-Stat1 signaling through IFN- α was shown to be important for the maturation, and specifically the engraftment potential of HSCs from the AUV into adult hosts (Kim et al., 2016); thus, inflammatory signaling is likely important during hematopoietic development from the emergence of pre-HSCs through their maturation into HSCs.

PD-L1 is expressed by antigen-presenting cells and functions to promote immune tolerance. The engagement of PD-L1 with its receptor, PD-1, expressed by T lymphocytes dampens the immune inhibitory response by suppressing T

cell self-renewal, inhibiting TCR-mediated IL-2 cytokine production by T cells, and activating T cell apoptosis (Carter et al., 2002; Chemnitz et al., 2004; Sheppard et al., 2004). It has been proposed that one reason embryonic HSCs are unable to engraft adult recipients is that they are immunologically distinct from adult HSCs and are recognized as foreign by the adult immune system, including T and NK cells (Kieusseian et al., 2012). PD-L1 was a logical candidate for suppressing the rejection of maturing embryonic HSCs by T lymphocytes in adult hosts, as it was shown that under some circumstances, PD-L1 can suppress graft rejection of adult HSCs in allogeneic transplants (Zheng et al., 2011). However, others (Zheng et al., 2011) and we have now shown that PD-L1:PD-1 signaling does not appear to be necessary for the engraftment of adult or embryonic HSCs in syngeneic hosts; hence, PD-L1 is a marker of, but not required for, HSC maturation.

MATERIALS AND METHODS

Mice

C57BL/6J WT (CD45.2) females were paired with B6.Cg-Tg(*Ly6a:GFP*)G5Dzk/J or C57BL/6 WT males to obtain conceptuses. The *Ly6a:GFP* transgene was detected by PCR using GFP primers: FW, 5'-CAGATGAAGCAGCAGCAC TTCT-3'; and RV, 5'-AACTCCAGCAGGACCATGTGAT-3'. The PCR reaction was as follows: denaturation 5 min 94°C, 35 cycles of denaturation 30 s 94°C, annealing 30 s 56°C, elongation 1 min and 30 s 72°C, and final extension 10 min 72°C. The product size was 400 bp. PD-1-null mice (*Pdcd1*^{tm1.15hr}) were a gift from A. Sharpe (Keir et al., 2007). NSG mice were provided by the University of Pennsylvania Stem Cell and Xenograft Core.

For transplantation assays, B6.SJL-*Ptprca*^a *Pepcb*^b/BoyJ (CD45.1), C57BL/6J (CD45.2), and PD-1-null (CD45.2) mice were subjected to a split dose of 900 cGy, 3 to 24 h apart. Recipients received 1–2 embryonic equivalents (ee) of E11.5 dissociated AUV cells plus 2 \times 10⁵ carrier spleen cells by tail vein injection. For Akt-EC coculture experiments, recipients received 1–2 ee of E10 to E11.5 AUV cocultured cells and 5 \times 10⁴ carrier CD45.1 BM cells by tail vein injection. E14.5 FL cell transplants into B6.SJL mice were performed with the following numbers of donor cells: IL7R⁺PD-L1^{+/-}, 10,000 cells; IL7R⁻PD-L1⁻, 53,000 cells; and IL7R⁻PD-L1⁺, 24,000 cells. Secondary transplants were performed by transplanting 2 \times 10⁶ unfractionated BM cells from primary hosts into irradiated secondary recipients. E11.5 and E12.5 FL cell transplants were performed with 0.5–2 ee. Donor fetuses were C57BL/6J for AUV-explant, AUV cultured on Akt-EC, direct AUV, and FL transplants, and a mixed C57BL/6J and 129S1/SVImJ background (CD45.2) for reaggregated populations. E14.5 transplants into NSG mice were performed with 20,000 donor cells into bisulfan-treated NSG mice. PD-1-null mice were given 1 AUV equivalent or 20,000 E14.5 FL B6.SJL donor cells. Donor engraftment was assessed after 3, 7, and 16 wk in the peripheral blood and after 16 wk in the BM.

All mouse experiments were approved by the University of Pennsylvania's Institutional Animal Care and Use Committee.

Cell sorting and flow cytometry

AUVs were dissociated using collagenase I (Sigma), filtered using a strainer cap (Becton Dickinson) and stained with appropriate antibodies in PBS/20% FBS/25 mM Hepes (Gibco) on ice. Cells were sorted on a BD FACSVantage, BD FACS Jazz, BD FACS Aria, or BD Influx using a 100- μ m nozzle, 15 psi pressure, flow rate <2,500 cells/s, and Hanks' balanced salt solution (Gibco)/25 mM Hepes (BD) as sheath fluid. Sorted cells were collected in 1.5-ml Eppendorf tubes or FACS tubes containing 0.5–3 ml PBS/50% FBS/25 mM Hepes. Post-sort analyses were performed when enough cells were available.

Antibodies used (RRID number) were CD144 (VEC; AB_10597442), CD45 (AB_465667), CD45.1 (AB_469628, AB_465675), CD45.2 (AB465060), CD117 (Kit; AB_1626278), Sca1 (893619), CD48 (AB_571997, AB_469407), CD150 (AB_439797), Ter119 (AB_1518808), Gr1 (AB_1548788, AB_1727563), Mac1 (AB_1582236, AB_2534404), CD19 (AB_1659676), B220 (AB_1645277, AB_1548761), CD3e (AB_1272193), CD25 (AB_830744), CD90.2 (AB_469642), CD274 (AB_466088, AB_397018), PD-1 (AB_465466), IL7R (AB_469435), and ESAM (AB_2101658, AB_891537). All samples were analyzed on an LSRII flow cytometer (BD).

Reaggregation and Akt-EC cultures

Sorted populations from one AUV were mixed with 10^5 OP9 cells as previously described (Taoudi et al., 2008; Rybtsov et al., 2011). The reaggregates were expelled onto 0.65- μ m Durapore filters (Millipore) and cultured at the air-liquid interface for 4 d in MyeloCult (M5300; STEMCELL Technologies) supplemented with 100 ng/ml stem cell factor, 100 ng/ml IL-3, and 100 ng/ml Flt3L (PeproTech). Reaggregates were dissociated using collagenase I (Sigma) before analysis. OP9 cells were obtained from the ATCC (CRL-2729) and maintained in α -Minimal Essential Medium (Gibco), 20% FBS (Gibco), and 1% penicillin-streptomycin (HyClone; Thermo Scientific). Cultures on Akt-EC cells were performed as described previously (Hadland et al., 2015).

Lymphoid assays

A limiting dilution range of FACS-sorted cell populations were cocultured on stromal cells for 10 d, as described previously (Li et al., 2014, 2017). OP9 or OP9-DL1 cells were seeded 1 d before coculture at 4,000 cells/well in 96-well tissue culture-treated plates (Falcon). For B cell potential, cells were cocultured on OP9 stroma in Alpha-MEM/20% FBS (Gibco) supplemented with 5 ng/ml mFlt3L and 10 ng/ml mIL7 (PeproTech). For T cell potential, cells were cocultured on OP9-DL1 stroma in Alpha-MEM/20% FBS supplemented with 5 ng/ml mFlt3L and 1 ng/ml mIL7. Progenitor frequencies were calculated using ELDA software (Hu and Smyth, 2009).

RNA purification and deep sequencing

Cells were sorted into Trizol-LS. Total RNA was prepared using an RNeasy micro kit (Qiagen). DNase treatment was performed either on-column (Qiagen) or using a DNA-free DNA Removal kit (Life Technologies). Total RNA was quantified with RNA HS kit (Q32852) for Qubit fluorometer (Life Technologies) and analyzed for integrity using an RNA 6000 Pico kit (5067–1513) for 2100 Bioanalyzer (Agilent). mRNA was isolated from total RNA using NEBNext Poly(A) mRNA Magnetic Isolation Module (E7490; NEB). PolyA-selected mRNA was fragmented to a mean size of 300 nt, reverse transcribed to generate double-stranded cDNA, and converted to a paired-end library using NEBNext Ultra RNA Library Prep kit for Illumina (E7530; NEB) according to the manufacturer's instructions, including the optional double size selection procedure using Agencourt AMPure XP beads. Prepared libraries were quantified with a dsDNA HS kit (Q32851) for Qubit, and the size distribution was assessed using a High Sensitivity DNA kit (5067-462) for Bioanalyzer. Libraries were sequenced on an Illumina HiSeq2500 in paired-end mode with the read length of 75 nt.

Transcriptome assembly and expression level estimate from read counts

Paired-end reads were mapped to the reference mouse genome (release mm9) using Tophat (Trapnell et al., 2009). Only uniquely mapped reads with fewer than two mismatches were used for downstream analyses. Transcripts were assembled using Cufflinks (Trapnell et al., 2009) using mapped fragments outputted by Tophat. Ensemble (release 66) was used as the source of annotated genes and transcript isoforms. Normalized transcript abundance was computed using Cufflinks and expressed as Fragments Per Kilobase of transcripts per Million mapped reads (FPKM). Gene-level FPKM values were computed by summing up FPKM values of their corresponding transcripts (Trapnell et al., 2010). RNA-Seq data reproducibility was assessed by computing Spearman correlation of gene expression between a pair of biological replicates. Genes with zero read counts in all biological replicates were excluded from the correlation calculation.

Identification of differentially expressed genes

FeatureCounts (Liao et al., 2014) was used to summarize read counts for genes. With normalized read counts for each gene, edgeR (Robinson and Oshlack, 2010) and DESeq (Anders and Huber, 2010) were applied to detect significantly differentially expressed genes for pairwise comparisons. Differentially expressed genes were determined by using a false discovery rate cutoff of 0.05 and a fold change of 2 for both algorithms.

PCA

Genes were ranked by the variance of their expression across samples. The top 5,000 genes with the largest variance were used for PCA.

GO enrichment analysis

Differentially expressed genes were used for enrichment analysis with level 5 GO terms. Enrichment p-values were computed using the hypergeometric distribution. Enrichment p-values were corrected for multiple testing using the Benjamini-Hochberg method (Benjamini and Hochberg, 1995).

Accession no.

The GEO accession no. for the RNA-Seq data is GSE104689.

Online supplemental information

Fig. S1 shows the quality of the RNA sequencing data and principal component analysis comparisons of pre-HSC, HSC^{ex}, and FL HSC. Fig. S2 shows the expression levels of gene clusters defined by consensus cluster analysis. Fig. S3 displays GO terms associated with specific expression clusters in comparison with each other. Fig. S4 displays engraftment data from HSC^{ex} secondary transplant recipients. Table S1, included as an Excel file, shows the genes in Clusters 1–6.

ACKNOWLEDGMENTS

We dedicate this work to Marijke Maijenburg, who died from acute myeloid leukemia during the revision of this manuscript. Marijke initiated these studies and continued to make major intellectual contributions up until the time of her death.

The research was supported by National Institutes of Health grants R01HL091724 (to N.A. Speck), U01HL100405NWO (to N.A. Speck and I.D. Bernstein), R21 HD081054 (to N.A. Speck and K. Tan), R01 HG006130 (to K. Tan), and R01 GM108716 (to K. Tan); the Leukemia and Lymphoma Society grant 3217-12 (to J. Tober); and NWO Rubicon grant 825.12.003 (to M.M.W. Maijenburg).

The authors declare no competing financial interests.

Author contributions: M.M.W. Maijenburg, Y. Li, J. Tober, K. Tan, and N.A. Speck designed the research and analyzed results; M.M.W. Maijenburg, J. Tober, B.K. Hadland, L. Gao, P. Gao, and K. Minoura performed experiments; and M.M.W. Maijenburg, J. Tober, K. Tan, I.D. Bernstein, and N.A. Speck wrote the manuscript.

Submitted: 22 September 2016

Revised: 6 October 2017

Accepted: 28 November 2017

REFERENCES

- Akashi, K., D. Traver, T. Miyamoto, and I.L. Weissman. 2000. A clonogenic common myeloid progenitor that gives rise to all myeloid lineages. *Nature*. 404:193–197. <https://doi.org/10.1038/35004599>
- Anders, S., and W. Huber. 2010. Differential expression analysis for sequence count data. *Genome Biol.* 11:R106. <https://doi.org/10.1186/gb-2010-11-10-r106>
- Benjamini, Y., and Y. Hochberg. 1995. Controlling the False Discovery Rate: A Practical and Powerful Approach to Multiple Testing. *J. R. Stat. Soc. Ser. A Stat. Soc.* 57:289–300.
- Bertrand, J.Y., N.C. Chi, B. Santoso, S. Teng, D.Y. Stainier, and D. Traver. 2010. Haematopoietic stem cells derive directly from aortic endothelium during development. *Nature*. 464:108–111. <https://doi.org/10.1038/nature08738>
- Böiers, C., J. Carrelha, M. Lutteropp, S. Luc, J.C. Green, E. Azzoni, P.S. Woll, A.J. Mead, A. Hultquist, G. Swiers, et al. 2013. Lymphomyeloid contribution of an immune-restricted progenitor emerging prior to definitive hematopoietic stem cells. *Cell Stem Cell*. 13:535–548. <https://doi.org/10.1016/j.stem.2013.08.012>
- Boisset, J.C., W. van Cappellen, C. Andrieu-Soler, N. Galjart, E. Dzierzak, and C. Robin. 2010. In vivo imaging of haematopoietic cells emerging from the mouse aortic endothelium. *Nature*. 464:116–120. <https://doi.org/10.1038/nature08764>
- Boisset, J.C., T. Clapes, A. Klaus, N. Papazian, J. Onderwater, M. Mommaas-Kienhuis, T. Cupedo, and C. Robin. 2015. Progressive maturation toward hematopoietic stem cells in the mouse embryo aorta. *Blood*. 125:465–469. <https://doi.org/10.1182/blood-2014-07-588954>
- Carter, L., L.A. Fouser, J. Jussif, L. Fitz, B. Deng, C.R. Wood, M. Collins, T. Honjo, G.J. Freeman, and B.M. Carreno. 2002. PD-1:PD-L inhibitory pathway affects both CD4(+) and CD8(+) T cells and is overcome by IL-2. *Eur. J. Immunol.* 32:634–643. [https://doi.org/10.1002/1521-4141\(200203\)32:3<634::AID-IMMU634>3.0.CO;2-9](https://doi.org/10.1002/1521-4141(200203)32:3<634::AID-IMMU634>3.0.CO;2-9)
- Chemnitz, J.M., R.V. Parry, K.E. Nichols, C.H. June, and J.L. Riley. 2004. SHP-1 and SHP-2 associate with immunoreceptor tyrosine-based switch motif of programmed death 1 upon primary human T cell stimulation, but only receptor ligation prevents T cell activation. *J. Immunol.* 173:945–954. <https://doi.org/10.4049/jimmunol.173.2.945>
- Chen, M.J., T. Yokomizo, B.M. Zeigler, E. Dzierzak, and N.A. Speck. 2009. Runx1 is required for the endothelial to haematopoietic cell transition but not thereafter. *Nature*. 457:887–891. <https://doi.org/10.1038/nature07619>
- de Bruijn, M.F., X. Ma, C. Robin, K. Ottersbach, M.J. Sanchez, and E. Dzierzak. 2002. Hematopoietic stem cells localize to the endothelial cell layer in the midgestation mouse aorta. *Immunity*. 16:673–683. [https://doi.org/10.1016/S1074-7613\(02\)00313-8](https://doi.org/10.1016/S1074-7613(02)00313-8)
- Eilken, H.M., S. Nishikawa, and T. Schroeder. 2009. Continuous single-cell imaging of blood generation from haemogenic endothelium. *Nature*. 457:896–900. <https://doi.org/10.1038/nature07760>
- Frame, J.M., K.H. Fegan, S.J. Conway, K.E. McGrath, and J. Palis. 2016. Definitive Hematopoiesis in the Yolk Sac Emerges from Wnt-Responsive Hemogenic Endothelium Independently of Circulation and Arterial Identity. *Stem Cells*. 34:431–444. <https://doi.org/10.1002/stem.2213>
- Gekas, C., F. Dieterlen-Lièvre, S.H. Orkin, and H.K. Mikkola. 2005. The placenta is a niche for hematopoietic stem cells. *Dev. Cell*. 8:365–375. <https://doi.org/10.1016/j.devcel.2004.12.016>
- Hadland, B.K., B. Varnum-Finney, M.G. Poulos, R.T. Moon, J.M. Butler, S. Rafii, and I.D. Bernstein. 2015. Endothelium and NOTCH specify and amplify aorta-gonad-mesonephros-derived hematopoietic stem cells. *J. Clin. Invest.* 125:2032–2045. <https://doi.org/10.1172/JCI80137>
- Holmes, C., and W.L. Stanford. 2007. Concise review: stem cell antigen-1: expression, function, and enigma. *Stem Cells*. 25:1339–1347. <https://doi.org/10.1634/stemcells.2006-0644>
- Hu, Y., and G.K. Smyth. 2009. ELDA: extreme limiting dilution analysis for comparing depleted and enriched populations in stem cell and other assays. *J. Immunol. Methods*. 347:70–78. <https://doi.org/10.1016/j.jim.2009.06.008>
- Kawamoto, H., T. Ikawa, K. Ohmura, S. Fujimoto, and Y. Katsura. 2000. T cell progenitors emerge earlier than B cell progenitors in the murine fetal liver. *Immunity*. 12:441–450. [https://doi.org/10.1016/S1074-7613\(00\)80196-X](https://doi.org/10.1016/S1074-7613(00)80196-X)
- Keir, M.E., G.J. Freeman, and A.H. Sharpe. 2007. PD-1 regulates self-reactive CD8+ T cell responses to antigen in lymph nodes and tissues. *J. Immunol.* 179:5064–5070. <https://doi.org/10.4049/jimmunol.179.8.5064>
- Kiel, M.J., O.H. Yilmaz, T. Iwashita, O.H. Yilmaz, C. Terhorst, and S.J. Morrison. 2005. SLAM family receptors distinguish hematopoietic stem and progenitor cells and reveal endothelial niches for stem cells. *Cell*. 121:1109–1121. <https://doi.org/10.1016/j.cell.2005.05.026>
- Kiusesian, A., P. Brunet de la Grange, O. Burlen-Defranoux, I. Godin, and A. Cumano. 2012. Immature hematopoietic stem cells undergo maturation

- in the fetal liver. *Development*. 139:3521–3530. <https://doi.org/10.1242/dev.079210>
- Kim, I., S. He, O.H. Yilmaz, M.J. Kiel, and S.J. Morrison. 2006. Enhanced purification of fetal liver hematopoietic stem cells using SLAM family receptors. *Blood*. 108:737–744. <https://doi.org/10.1182/blood-2005-10-4135>
- Kim, P.G., M.C. Canver, C. Rhee, S.J. Ross, J.V. Harriss, H.C. Tu, S.H. Orkin, H.O. Tucker, and G.Q. Daley. 2016. Interferon- α signaling promotes embryonic HSC maturation. *Blood*. 128:204–216. <https://doi.org/10.1182/blood-2016-01-689281>
- Kissa, K., and P. Herbomel. 2010. Blood stem cells emerge from aortic endothelium by a novel type of cell transition. *Nature*. 464:112–115. <https://doi.org/10.1038/nature08761>
- Kobayashi, H., J.M. Butler, R. O'Donnell, M. Kobayashi, B.S. Ding, B. Bonner, V.K. Chiu, D.J. Nolan, K. Shido, L. Benjamin, and S. Rafii. 2010. Angiocrine factors from Akt-activated endothelial cells balance self-renewal and differentiation of haematopoietic stem cells. *Nat. Cell Biol.* 12:1046–1056. <https://doi.org/10.1038/ncb2108>
- Kondo, M., I.L. Weissman, and K. Akashi. 1997. Identification of clonogenic common lymphoid progenitors in mouse bone marrow. *Cell*. 91:661–672. [https://doi.org/10.1016/S0092-8674\(00\)80453-5](https://doi.org/10.1016/S0092-8674(00)80453-5)
- Kumaravelu, P., L. Hook, A.M. Morrison, J. Ure, S. Zhao, S. Zuyev, J. Ansell, and A. Medvinsky. 2002. Quantitative developmental anatomy of definitive haematopoietic stem cells/long-term repopulating units (HSC/RUs): role of the aorta-gonad-mesonephros (AGM) region and the yolk sac in colonisation of the mouse embryonic liver. *Development*. 129:4891–4899.
- Lancrin, C., P. Sroczyńska, C. Stephenson, T. Allen, V. Kouskoff, and G. Lacaud. 2009. The haemangioblast generates haematopoietic cells through a haemogenic endothelium stage. *Nature*. 457:892–895. <https://doi.org/10.1038/nature07679>
- Lee, S.J., B.C. Jang, S.W. Lee, Y.I. Yang, S.I. Suh, Y.M. Park, S. Oh, J.G. Shin, S. Yao, L. Chen, and I.H. Choi. 2006. Interferon regulatory factor-1 is prerequisite to the constitutive expression and IFN- γ -induced upregulation of B7-H1 (CD274). *FEBS Lett.* 580:755–762. <https://doi.org/10.1016/j.febslet.2005.12.093>
- Li, Y., V. Esain, L. Teng, J. Xu, W. Kwan, I.M. Frost, A.D. Yzaguirre, X. Cai, M. Cortes, M.W. Majtenburg, et al. 2014. Inflammatory signaling regulates embryonic hematopoietic stem and progenitor cell production. *Genes Dev.* 28:2597–2612. <https://doi.org/10.1101/gad.253302.114>
- Li, Y., L. Gao, B. Hadland, K. Tan, and N.A. Speck. 2017. CD27 marks murine embryonic hematopoietic stem cells and type II prehematopoietic stem cells. *Blood*. 130:372–376. <https://doi.org/10.1182/blood-2017-03-776849>
- Liao, Y., G.K. Smyth, and W. Shi. 2014. featureCounts: an efficient general purpose program for assigning sequence reads to genomic features. *Bioinformatics*. 30:923–930. <https://doi.org/10.1093/bioinformatics/btt656>
- McKinney-Freeman, S.L., O. Naveiras, F. Yates, S. Loewer, M. Philitas, M. Curran, P.J. Park, and G.Q. Daley. 2009. Surface antigen phenotypes of hematopoietic stem cells from embryos and murine embryonic stem cells. *Blood*. 114:268–278. <https://doi.org/10.1182/blood-2008-12-193888>
- Medvinsky, A., and E. Dzierzak. 1996. Definitive hematopoiesis is autonomously initiated by the AGM region. *Cell*. 86:897–906. [https://doi.org/10.1016/S0092-8674\(00\)80165-8](https://doi.org/10.1016/S0092-8674(00)80165-8)
- Müller, A.M., A. Medvinsky, J. Strouboulis, F. Grosveld, and E. Dzierzak. 1994. Development of hematopoietic stem cell activity in the mouse embryo. *Immunity*. 1:291–301. [https://doi.org/10.1016/1074-7613\(94\)90081-7](https://doi.org/10.1016/1074-7613(94)90081-7)
- North, T.E., M.F. de Bruijn, T. Stacy, L. Talebian, E. Lind, C. Robin, M. Binder, E. Dzierzak, and N.A. Speck. 2002. Runx1 expression marks long-term repopulating hematopoietic stem cells in the midgestation mouse embryo. *Immunity*. 16:661–672. [https://doi.org/10.1016/S1074-7613\(02\)00296-0](https://doi.org/10.1016/S1074-7613(02)00296-0)
- Riella, L.V., A.M. Paterson, A.H. Sharpe, and A. Chandraker. 2012. Role of the PD-1 pathway in the immune response. *Am. J. Transplant.* 12:2575–2587. <https://doi.org/10.1111/j.1600-6143.2012.04224.x>
- Robinson, M.D., and A. Oshlack. 2010. A scaling normalization method for differential expression analysis of RNA-seq data. *Genome Biol.* 11:R25. <https://doi.org/10.1186/gb-2010-11-3-r25>
- Rybtsov, S., M. Sobiesiak, S. Taoudi, C. Souilhoul, J. Senserrich, A. Liakhovitskaia, A. Ivanovs, J. Frampton, S. Zhao, and A. Medvinsky. 2011. Hierarchical organization and early hematopoietic specification of the developing HSC lineage in the AGM region. *J. Exp. Med.* 208:1305–1315. <https://doi.org/10.1084/jem.20102419>
- Rybtsov, S., A. Batsivari, K. Bilotkach, D. Paruzina, J. Senserrich, O. Nerushev, and A. Medvinsky. 2014. Tracing the origin of the HSC hierarchy reveals an SCF-dependent, IL-3-independent CD43(-) embryonic precursor. *Stem Cell Reports*. 3:489–501. <https://doi.org/10.1016/j.stemcr.2014.07.009>
- Rybtsov, S., A. Ivanovs, S. Zhao, and A. Medvinsky. 2016. Concealed expansion of immature precursors underpins acute burst of adult HSC activity in foetal liver. *Development*. 143:1284–1289. <https://doi.org/10.1242/dev.131193>
- Sánchez, M.-J., A. Holmes, C. Miles, and E. Dzierzak. 1996. Characterization of the first definitive hematopoietic stem cells in the AGM and liver of the mouse embryo. *Immunity*. 5:513–525. [https://doi.org/10.1016/S1074-7613\(00\)80267-8](https://doi.org/10.1016/S1074-7613(00)80267-8)
- Sawamiphak, S., Z. Kontarakis, and D.Y. Stainier. 2014. Interferon gamma signaling positively regulates hematopoietic stem cell emergence. *Dev. Cell*. 31:640–653. <https://doi.org/10.1016/j.devcel.2014.11.007>
- Sheppard, K.A., L.J. Fitz, J.M. Lee, C. Benander, J.A. George, J. Wooters, Y. Qiu, J.M. Jussif, L.L. Carter, C.R. Wood, and D. Chaudhary. 2004. PD-1 inhibits T-cell receptor induced phosphorylation of the ZAP70/CD3zeta signalosome and downstream signaling to PKC θ . *FEBS Lett.* 574:37–41. <https://doi.org/10.1016/j.febslet.2004.07.083>
- Taoudi, S., A.M. Morrison, H. Inoue, R. Gribi, J. Ure, and A. Medvinsky. 2005. Progressive divergence of definitive haematopoietic stem cells from the endothelial compartment does not depend on contact with the foetal liver. *Development*. 132:4179–4191. <https://doi.org/10.1242/dev.01974>
- Taoudi, S., C. Gonneau, K. Moore, J.M. Sheridan, C.C. Blackburn, E. Taylor, and A. Medvinsky. 2008. Extensive hematopoietic stem cell generation in the AGM region via maturation of VE-cadherin+CD45+ pre-definitive HSCs. *Cell Stem Cell*. 3:99–108. <https://doi.org/10.1016/j.stem.2008.06.004>
- Trapnell, C., L. Pachter, and S.L. Salzberg. 2009. TopHat: discovering splice junctions with RNA-Seq. *Bioinformatics*. 25:1105–1111. <https://doi.org/10.1093/bioinformatics/btp120>
- Trapnell, C., B.A. Williams, G. Pertea, A. Mortazavi, G. Kwan, M.J. van Baren, S.L. Salzberg, B.J. Wold, and L. Pachter. 2010. Transcript assembly and quantification by RNA-Seq reveals unannotated transcripts and isoform switching during cell differentiation. *Nat. Biotechnol.* 28:511–515. <https://doi.org/10.1038/nbt.1621>
- Yokomizo, T., and E. Dzierzak. 2010. Three-dimensional cartography of hematopoietic clusters in the vasculature of whole mouse embryos. *Development*. 137:3651–3661. <https://doi.org/10.1242/dev.051094>
- Zheng, J., M. Umikawa, S. Zhang, H. Huynh, R. Silvano, B.P. Chen, L. Chen, and C.C. Zhang. 2011. Ex vivo expanded hematopoietic stem cells overcome the MHC barrier in allogeneic transplantation. *Cell Stem Cell*. 9:119–130. <https://doi.org/10.1016/j.stem.2011.06.003>
- Zhou, F., X. Li, W. Wang, P. Zhu, J. Zhou, W. He, M. Ding, F. Xiong, X. Zheng, Z. Li, et al. 2016. Tracing haematopoietic stem cell formation at single-cell resolution. *Nature*. 533:487–492. <https://doi.org/10.1038/nature17997>

Zovein, A.C., J.J. Hofmann, M. Lynch, W.J. French, K.A. Turlo, Y. Yang, M.S. Becker, L. Zanetta, E. Dejana, J.C. Gasson, et al. 2008. Fate tracing reveals

the endothelial origin of hematopoietic stem cells. *Cell Stem Cell*. 3:625–636. <https://doi.org/10.1016/j.stem.2008.09.018>